RESEARCH ARTICLE | APRIL 22 2021

Ultra-stable 1064-nm neodymium-doped yttrium aluminum garnet lasers with 2.5 × 10^{-16} frequency instability

Liufeng Li ✉; Jia Wang; Jin Bi; Tao Zhang; Jiankang Peng; Yunlin Zhi; Lisheng Chen ✉

Rev. Sci. Instrum. 92, 043001 (2021)
https://doi.org/10.1063/5.0025498

Review of Scientific Instruments ARTICLE scitation.org/journal/rsi

Ultra-stable 1064-nm neodymium-doped yttrium aluminum garnet lasers with 2.5×10^{-16} frequency instability

Cite as: Rev. Sci. Instrum. 92, 043001 (2021); doi: 10.1063/5.0025498
Submitted: 16 August 2020 • Accepted: 5 April 2021 •
Published Online: 22 April 2021

Liufeng Li,[1,2,3] Jia Wang,[1,4] Jin Bi,[1,2,3] Tao Zhang,[1,4] Jiankang Peng,[1,4] Yunlin Zhi,[1,4] and Lisheng Chen[1,2,3,4,a)]

AFFILIATIONS

[1] Innovation Academy for Precision Measurement Science and Technology, Chinese Academy of Sciences, Wuhan 430071, China
[2] State Key Laboratory of Magnetic Resonance and Atomic and Molecular Physics, Wuhan 430071, China
[3] Laboratory of Atomic Frequency Standards, Chinese Academy of Sciences, Wuhan 430071, China
[4] University of Chinese Academy of Sciences, Beijing 100080, China

[a)] **Author to whom correspondence should be addressed:** lchen@wipm.ac.cn

ABSTRACT

Cavity-stabilized ultra-stable optical oscillators are one of the core ingredients in the ground-based or spaceborne precision measurements such as optical frequency metrology, test of special relativity, and gravitational wave observation. We report in detail the development of two ultra-stable systems based on 1064-nm neodymium-doped yttrium aluminum garnet lasers and 20-cm optical cavities. The optical cavities adopt ultra-low-loss silica mirrors with compensating rings. An electro-optic crystal with a wedged angle is used to reduce the residual amplitude modulation. Using two-stage thermal control, long-term stabilities of 100 μK are achieved for the outer wall of the vacuum chamber housing the optical cavity. Two additional thermal shields increased the time constant of the optical cavities to 70 h. By operating the optical cavity at the temperature of zero coefficient of thermal expansion, the frequency stability reaches 2.5×10^{-16} at 10 s averaging time and remains below 5×10^{-16} with an extended time of 1000 s after removing the first- and second-order drifts. The dependence of the laser linewidth on the measurement time is tested against a simplified theoretical model.

I. INTRODUCTION

Ultra-stable lasers[1–11] contributed greatly to the advancement of optical frequency standards with stabilities of 10^{-18} to 10^{-19}.[12–14] In an optical frequency standard, a clock laser is frequency stabilized by using an ultra-stable optical cavity, serving as a local oscillator to probe the clock transitions in cold neutral atoms[14] or trapped single ion.[13] Increasing the frequency stability of the optical oscillator in time scales from 1 s to 1000 s is one of the crucial tasks in optical-clock-related research as well as many precision measurements, such as gravitational-wave detection[15–21] and testing Lorentz invariance.[22–24]

The stability of cavity-stabilized lasers is limited by thermal noise in the optical cavity[25] and other sources such as environmental perturbations. For lasers stabilized by room-temperature optical cavities with a length of 10 cm, the frequency instability can be reduced to (5–6) $\times 10^{-16}$ at averaging times of 1–10 s.[26] The thermal noise (or its influence) can be reduced by using a longer cavity and adopting mirror coatings and substrates with lower mechanical loss.[25] Increasing the size of the beam spot on the mirrors can also reduce the effect of the thermal noise, as can be realized by either using high-order cavity modes[11,27] or mirrors with a large radius of curvature (ROC). In addition, crystalline coatings with lower thermal noise have been successfully developed and applied to ultra-low loss optical cavities.[28,29]

The thermal-fluctuation induced cavity instability is one of the major noise contributors and is especially prominent at averaging times beyond a few tens of seconds.[30] Optical cavities made of a special material, e.g., Corning ultra-low expansion (ULE) glass, exhibit a zero coefficient of thermal expansion at a certain transition temperature T_c. By operating the optical cavity near T_c, the long-term stability can be dramatically improved.[3] The present room-temperature systems adopting aforementioned measures have achieved 10^{-16} to 10^{-17} level frequency stabilities.[6,7,10,11] Materials such as crystalline silicon or sapphire have low mechanical loss and have their T_c at cryogenic temperatures.[31] Lasers locked to silicon cavities operating

at either 124 or 4 K are already highly promising for both short and long-term stabilities.[8,9]

As an indispensable step toward developing ultra-stable lasers for precision measurements, we developed two cavity-stabilized 1064-nm neodymium-doped yttrium aluminum garnet (Nd:YAG) lasers with a nonplanar-ring-oscillator (NPRO) configuration, aiming at the 10^{-16} level frequency stability with improved long-term performance. To increase the frequency stability, the cavity length is increased from 10 to 20 cm, and silica mirror substrates with ULE compensating rings are used instead of ULE mirrors. In addition, the vibration sensitivity of the optical cavity is minimized with the help of finite element analysis (FEA).[26,32–34] We also adopt an electro-optic modulator (EOM)[35–38] with reduced residual amplitude modulation (RAM). To improve the thermal stability of the optical cavity, which is usually the dominate source of the frequency drift at time scales beyond a few tens of seconds, the vacuum chamber is equipped with multi-layer thermal shields and the optical cavity is operated close to its T_c. The performance is evaluated by beating the two lasers independently locked to 20-cm optical cavities. In addition, the linewidth of the cavity-stabilized laser is measured with different sampling times and the result is compared with the predication of a model[39] that shows a simplified relationship between the linewidth of an oscillator and its frequency noise.

II. PDH LASER FREQUENCY LOCKING

Figure 1 shows the experimental setup for our cavity-stabilized system, which consists of a nonplanar-ring-oscillator (NPRO) Nd:YAG laser locked to an optical cavity using the Pound–Drever–Hall (PDH) method.[40] Two identical ultra-stable systems (WEST and EAST) are constructed and their heterodyne beat is used for performance evaluation and optimization.

As shown in Fig. 1, the glass windows on the vacuum chamber and the outer thermal shield are tilted by 5° to avoid interference between the incoming and reflected beams. There is no window on the inner thermal shield, and the laser passes through a hole on the shield and hits upon the optical cavity. The pressure inside the vacuum is ~3×10^{-5} Pa, which is maintained by two 15-L/s ion pumps (JJJvac SP-15).

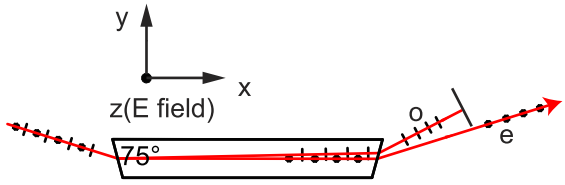

FIG. 2. EOM crystal with wedged end surfaces. After passing the crystal, only the e component is used for PDH frequency locking, avoiding the amplitude modulation caused by the crystal birefringence.

The modulation frequencies of the two EOMs in the WEST and EAST systems are 12.288 and 10 MHz, respectively. The laser frequency is corrected by a piezo-electric transducer (PZT) with an actuating bandwidth on the order of a few kHz and by additionally adjusting the temperature of the NPRO on time scales longer than 10 s. Fiber noise cancellation[41] is employed to suppress the phase noise induced by the optical fiber that transmits light from the optical bench to the top of vibration isolation platforms on which the optical cavity and PDH locking optics locate. The intensity of the light reflected by the polarization beam splitter (PBS) before the optical cavity is stabilized by adjusting the driving power of an acousto-optic modulator (AOM) used for the fiber noise cancellation.

We adopt a specially designed EOM[35–38] to suppress the RAM arising from the birefringence of the EOM crystal.[42–45] Figure 2 shows the details of the EOM crystal, which is made of magnesium doped lithium niobate ($MgO{\cdot}LiNbO_3$). The input and output facets of the crystal are beveled, and its principal axis is along the z direction. As the e (extraordinary) and o (ordinary) lights travel through the crystal, they are spatially separated, and only the e component is used for PDH frequency locking, eliminating the interference of the two components whose phase differences is sensitive

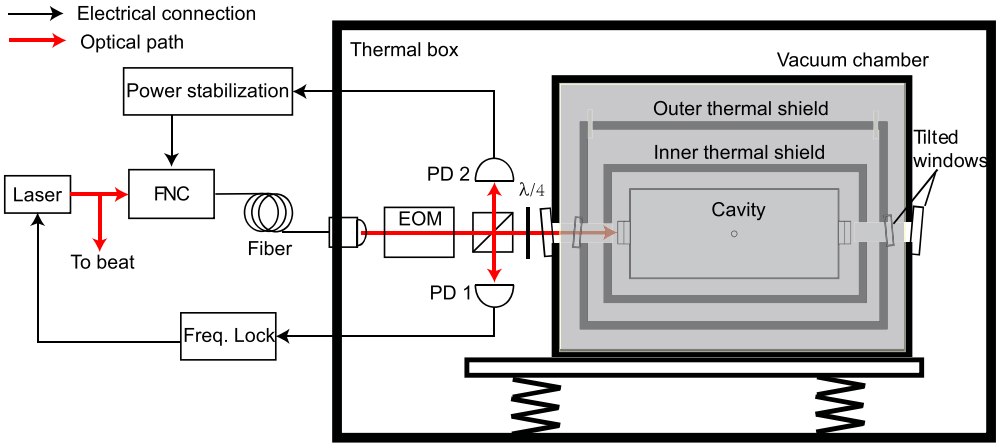

FIG. 1. Experimental setup for two ultra-stable 1064 nm Nd:YAG lasers. FNC—fiber noise cancellation, EOM—electro-optic modulator, PD—photodetector, and λ/4—quarter wave plate.

to environmental perturbations. Active control of the RAM[30] is not needed with the new EOM, and it shows a reduced susceptibility to input polarization, backscattered light, and the fluctuation of ambient temperature.

III. 20-cm OPTICAL CAVITY WITH REDUCED VIBRATION SENSITIVITY

A. Geometric and optical parameters

A longer optical cavity helps in reducing the influence of the thermal noise, but it increases the volume, weight, and cost of the entire system. Based on trade-offs among these competing factors, 20-cm optical cavities are chosen for a targeted stability on the level of 2×10^{-16}. Figure 3 shows the optical cavity and its supporting structure. Mirror substrates made of silica are used to directly reduce the thermal noise.[25] A ULE ring is attached to the outer side of the silica mirror to compensate the change in T_c caused by the stress developed in the ULE–silica interface on the end face of the ULE spacer.[46,47] Similar to its 10-cm counterpart,[30] the 20-cm optical cavity uses flat and concave mirrors, except that the radius of curvature (ROC) of the concave mirror is increased from 0.5 to 1 m. Accordingly, the spot size of the TEM_{00} mode inside the cavity is enlarged from 0.26 (0.29) to 0.37 (0.41) mm on the flat (concave) mirror. The combined effect of a doubled cavity length, silica mirror substrates instead of ULE ones, and a larger beam spot size will provide about fivefold improvement on the stability, reducing the thermal-noise-limited frequency instability from 7.0×10^{-16} of the 10-cm optical cavity to 1.5×10^{-16}.

TABLE I. Parameters of the two 20-cm optical cavities.

	EAST	WEST
Length	20 cm	20 cm
Mirror ROC	Flat/1 m	Flat/1 m
Finesse	495 000	443 000
Mirror transmission[a] (T_m)	3.1 ppm	2.7 ppm
Mirror loss[a] (L_m)	3.2 ppm	4.4 ppm

[a]Values are for a single mirror (assuming that the two mirrors of the cavity have the same transmission and loss).

The finesse of the cavity is measured with the cavity ring-down technique.[48,49] To measure the loss of the cavity, the two optical-power ratios, i.e., the reflection and transmission to the incidence, are measured by sweeping the laser frequency across a TEM_{00} resonance of the cavity. By assuming that the two mirrors have identical properties, the transmission T_m and loss L_m of each mirror are deduced from the finesse and the two power ratios.[50] The results are listed in Table I for the EAST and WEST cavities along with their geometric parameters.

B. Acceleration sensitivity

Finite element analysis (FEA) is used to reduce the susceptibility of the optical cavity to vibration perturbations.[26,32–34] The parameter H of the notch and the distance D of the two Viton spheres (c.f. Fig. 3) are varied to minimize the acceleration sensitivity in the vertical direction. Presently, a full optimization is not available because

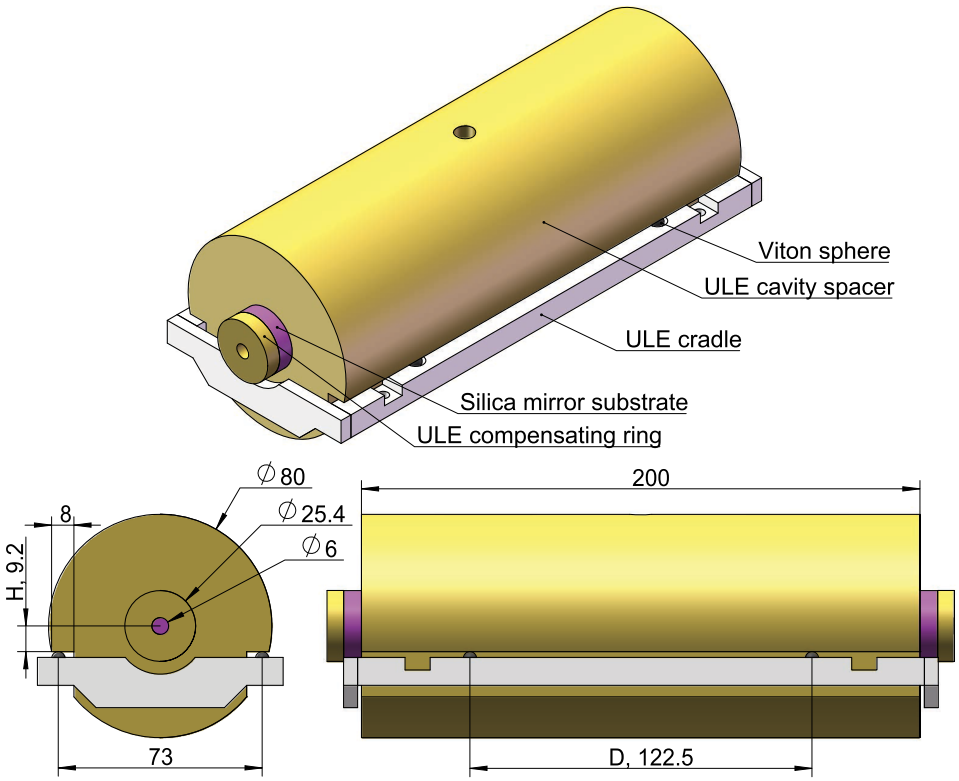

FIG. 3. CAD drawing of the optical cavity. A ULE ring is attached to the fused-silica mirror substrate to compensate the change in the T_c of the optical cavity. The optical cavity is support by four Viton spheres located on a ULE cradle that is fixed on the inner thermal shield. Dimensions are in mm. The diameters of the Viton spheres and the central through hole are 4.76 and 11 mm, respectively.

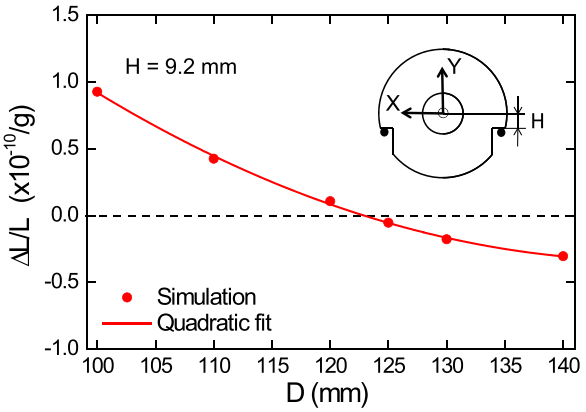

FIG. 4. Simulated acceleration sensitivity in the vertical direction. Inset shows the front view of the cavity (with the flat mirror exposed) and the coordinate system used in FEA. The acceleration (9.81 m/s^2) is applied along the opposite direction of the Y axis. L and ΔL are the original length and its variation due to the acceleration, respectively.

the convergent solution cannot be obtained for horizontal accelerations. At the optimized notch parameter of $H = 9.2$ mm, Fig. 4 shows the simulated acceleration sensitivity in the vertical direction. In the simulation, the Viton spheres are modeled as ideal elastic solid (elastic modules—7.84×10^6 Pa, Poisson ratio—0.47, and density—1.82×10^3 kg/m^3), non-penetration is enforced at the sphere-spacer contact, and the surface of the lower half hemisphere of the Viton sphere is fixed in X (transverse), Y (vertical), and Z (axial) directions.

The acceleration sensitivities of two optical cavities are measured in X, Y, and Z directions. One laser is locked to an optical cavity serving as a frequency reference, while the second laser is locked to the optical cavity whose sensitivity is to be measured. At a frequency of 5 Hz, a sinusoidal varying force shakes the vibration isolation platform on which the optical cavity under test is installed and the heterodyne beat of the two lasers is recorded. The acceleration sensitivity is obtained by dividing the frequency variation at the driving frequency by the acceleration registered by a sensor on the platform. Table II lists the experimentally determined acceleration sensitivities of two optical cavities.

IV. THERMAL STABILITY OF THE OPTICAL CAVITY

Three measures are combined to reduce the influence of the temperature fluctuation on the stability of the optical cavity. First, the vacuum chamber is temperature controlled with the stability of ~100 μK. Second, two thermal shields are added in the vacuum chamber, increasing the thermal time constant of the optical cavity from ~8 to >70 h. Finally, the temperature of the optical cavity is maintained close to its zero-expansion temperature T_c, which is slightly above the room temperature.

TABLE II. Acceleration sensitivities of the two 20-cm optical cavities.

Direction	Cavity EAST	Cavity WEST
Horizontal, axial (1/g)	2.32×10^{-10}	4.35×10^{-10}
Horizontal, transverse (1/g)	5.2×10^{-11}	5.8×10^{-11}
Vertical (1/g)	2.9×10^{-11}	1.45×10^{-10}

A. Thermal stability of the vacuum chamber

A two-stage thermal control is adopted in the current system.[30] As depicted in Fig. 1, the vacuum chamber housing the optical cavity, together with the frequency-locking optics and vibration isolation stage, is enclosed by a sealed thermal box built of aluminum plates, which are temperature controlled using Kapton heating foils attached to the inner surfaces of the plates. Furthermore, Kapton heating foils are applied to about 80% of the surface area of the vacuum chamber whose cylindrical wall and two end caps are independently temperature controlled. For this purpose, three pairs of thermistors (44008RC) are installed on the middle of the cylindrical wall and at the edges of two end caps, respectively.

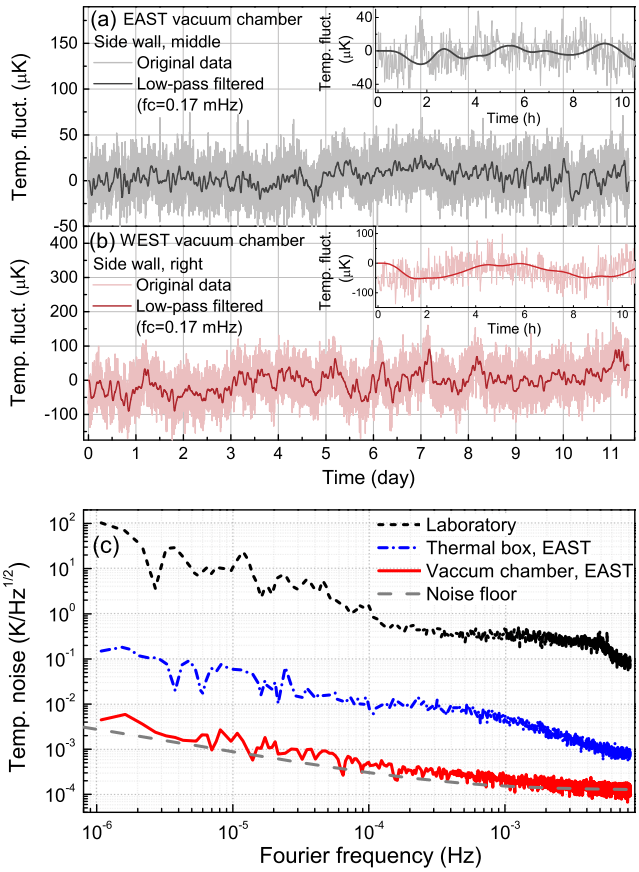

FIG. 5. Two-stage temperature stabilization of the vacuum chamber housing the optical cavity. Temperature fluctuations of the (a) EAST and (b) WEST vacuum chambers. (c) Noise spectral densities of the temperature fluctuations at various locations. Insets examine temperature fluctuations in a 10-h duration. The time series (light tone) are measured by using digital multimeters with a sampling rate of 1/(60 s) and integration times of 2 s (EAST) and 1.2 s (WEST). The measured temperature fluctuations are digitally low-pass filtered with 0.17 mHz corner frequency and superimposed on the original ones. The vacuum chamber is inside a sealed thermal box made of aluminum plates. The dashed curve at the bottom is the measured noise of the DMM, which is used for the out-of-loop measurement.

The two thermistors of each pair are separated by 3.5 mm; one is used for temperature control and the other performs out-of-loop measurement.

Figure 5 shows the temperature fluctuations of two vacuum chambers as well as the noise spectra of temperature fluctuations measured at various locations. In a period of 11 days, the thermal stabilities of the two vacuum chambers are 100–200 μK. As shown in Fig. 5(c), the noise spectrum measured at the vacuum chamber is approaching the noise floor contributed by the digital multimeter (DMM) that measures the resistance of the out-of-loop thermistor, indicating that the temperature fluctuations observed on the vacuum chamber are mostly due to excess electronic noise of the out-of-loop measurement.

B. Time constant of the optical cavity

In addition to improving the thermal stability of the vacuum chamber, limiting the rate of the heat exchange between the vacuum chamber and optical cavity is an effective way to filter out slow-varying fluctuations, thereby increasing the long-term stability of the optical cavity.

Figures 6(a) and 6(b) illustrate the two layers of the thermal shield that are added to the vacuum chamber. The step responses of two thermal shields and the optical cavity are measured and shown in Fig. 7. Before measurement, the temperature of the vacuum chamber is maintained at ~90 °C and the system reaches thermal equilibrium. The heating is then stopped and forced cooling is performed to bring the temperature of the vacuum chamber rapidly down to room temperature within 1 h. As the temperature of the vacuum chamber is settled down and then stabilized to 20 °C, the responses of the thermal shields and the cavity are measured. The fitted time constants of the two optical cavities are 87 and 70 h, respectively. These values give a quantitative evaluation of how fast the cavities respond to external thermal perturbations.

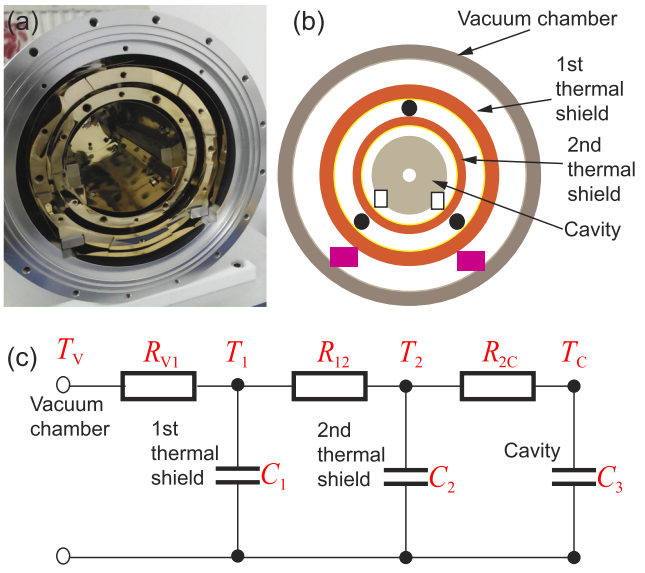

FIG. 6. Multi-layer thermal shield between the optical cavity and the vacuum chamber. (a) Photograph of the vacuum chamber. (b) Multi-layer structure. (c) The electrically equivalent model of the heat exchange of the multi-layer structure of the vacuum chamber and the optical cavity. The thermal shields are made of copper coated with gold to minimize the thermal radiation. Adjacent layers are separated by steel balls and/or Teflon pads to reduce the thermal conduction.

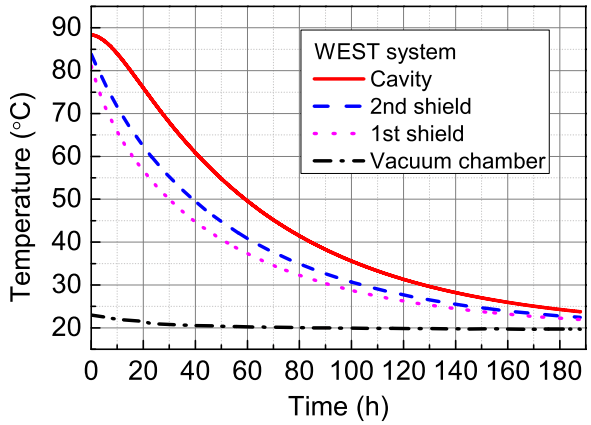

FIG. 7. Step responses of the vacuum chamber, the thermal shields, and the optical cavity. The results shown are for the WEST system, and the other system (EAST) shows similar responses. The fitted effective time constants of the cavities are 70 (WEST) and 87 (EAST) h.

C. Measurement of T_c

The T_c of the optical cavity is determined by optical heterodyne beat between the two cavity-locked lasers. While the reference cavity is temperature stabilized, the temperature of the vacuum chamber housing the optical cavity under test is swept up and then down during which the beat of the two lasers is recorded and the temperature

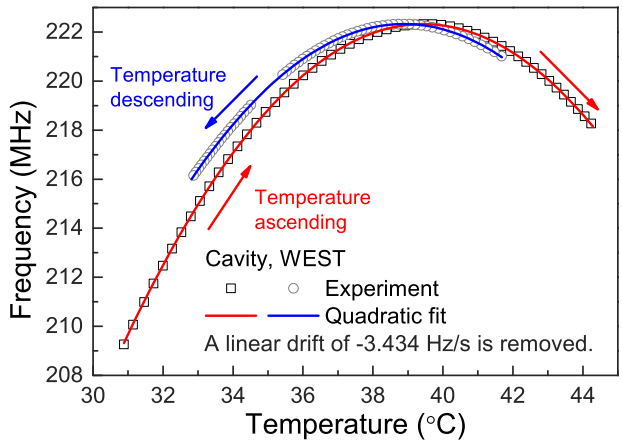

FIG. 8. The bi-directional temperature sweep for determining T_c of an optical cavity (WEST). The cavity temperature is swept upward and then downward. Quadratic fits are performed to find the two turning points whose average is used as the T_c of the optical cavity.

TABLE III. Zero-expansion temperatures (T_c) and linear temperature coefficients (k) of the two 20-cm optical cavities.

	Cavity EAST	Cavity WEST
T_c (°C)	31.57 (12)	39.16 (16)
k (1/K^2)	5.6×10^{-10}	6.3×10^{-10}

of the optical cavity is measured by a platinum resistance attached to the cavity spacer.

Figure 8 shows the beat frequencies during the temperature sweeps of the WEST cavity. Quadratic fits are separately performed for the heating and cooling phases, yielding two temperature turning points whose average is used for the T_c of the optical cavity. The measured temperatures of zero thermal-expansion coefficient are 31.57(12) and 39.16(16) °C for the EAST and WEST cavities, respectively, where the uncertainties account for the difference between the two turning points of the heating and cooling phases. The linear temperature coefficients k, i.e., the slope of the thermal expansion coefficient at T_c, are also determined from the quadratic fits and are given in Table III. After the measurement, the temperature of the vacuum chamber is adjusted and stabilized to the measured zero-coefficient temperature of the optical cavity.

D. Thermal stability of the optical cavity

To analyze how the temperature fluctuations of the vacuum chamber affect the stability of the optical cavity, the multi-layer structure is modeled by taking an analogy to three electronic low-pass filters connected in series.[51] Figure 6(c) shows this electrically equivalent model, and the parameters of each filter, given in Table IV, are determined by the measured time responses (c.f. Fig. 7) and the heat capacitances of the layers involved. Note that this RC-network model is valid only when the temperature differences among various layers inside the vacuum chamber are small enough to allow for a linear approximation on the rate of the heat transfer through thermal radiation.

With the temperature measured on the vacuum chamber as the input, the electrically equivalent model is used to calculate the thermal fluctuation of the optical cavity. At a certain temperature near T_c, the thermal fluctuation of the cavity is converted to frequency instability according to the linear temperature coefficient given in Table III. When the cavity temperature is within the range of $T_c \pm 0.2$ K, the frequency instability arising from the temperature fluctuation of the vacuum chamber is less than 1×10^{-17} at averaging times up to 1000 s, and the thermal excursions of the optical cavity are on the order of a few μK and exhibit periods of a few hours. If the tolerance on T_c is relaxed from 0.2 to 1 K, the calculated frequency instability is still below 1×10^{-16} at the same time scales.

TABLE IV. Parameters in the thermal model characterizing the optical cavity and multi-layer structure shown in Fig. 6.

	EAST	WEST
C_1 (J/K)	4.21×10^3	3.71×10^3
C_2 (J/K)	3.07×10^3	2.40×10^3
C_3 (J/K)	2.04×10^3	2.04×10^3
R_{V1} (K/W)	12.99	19.70
R_{12} (K/W)	32.57	6.71
R_{2C} (K/W)	17.30	28.92

V. FREQUENCY STABILITY

To evaluate the frequency stability of the current system, each Nd:YAG laser is locked to its own 20-cm optical cavity. The heterodyne beat between two locked lasers is down converted and measured by a frequency counter. The beat exhibits a linear drift on the order of 0.034 Hz/s on a daily basis. Figure 9(a) shows a 300-min time series of the beat note with this linear drift removed, and in Fig. 9(b), a second-order drift is further removed. Allan deviations are computed for averaging times from 0.1 to 1000 s and shown in Fig. 9(c). Figure 10 shows the noise spectrum of the beat as well as the contribution from the thermal noise[25] of the two optical cavities. The frequency instability of the heterodyne beat is reduced to 3.5×10^{-16} (2.5×10^{-16}, a single laser) around 1 s, below which the detection noise starts to dominate. After removing the first- and second-order drifts, the instability of the beat remains below 7×10^{-16} (5×10^{-16}, a single laser) at averaging times up to 1000 s. Currently, two noise contributors, the pressure fluctuation of the residual gas and the laser intensity noise, prevent the instability of a single laser being further reduced down to the thermal-noise-limited value of 1.5×10^{-16}.

In a previous work,[30] the linewidths of a radio-frequency (RF) oscillator and a cavity-stabilized laser are measured to verify a model[39] that shows a simplified relationship between the spectral linewidth of an oscillator and its frequency noise. A similar measurement is also performed on current lasers with upgraded frequency stability. The linewidth of the beat note between the two lasers is

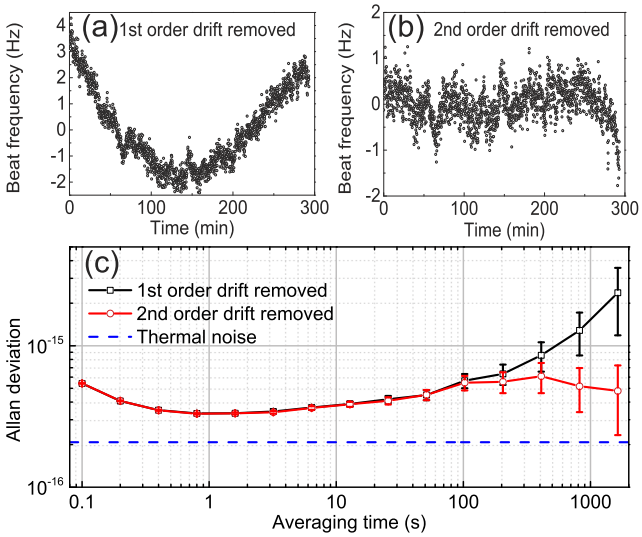

FIG. 9. Frequency instability of the two Nd:YAG lasers independently locked to two 20-cm cavities. A 300-min time series of the down-converted beat frequency when (a) the first-order (linear) drift is removed and (b) both the first- and second-order drifts are removed. (c) The corresponding Allan deviations and contribution from the thermal noise of two optical cavities.

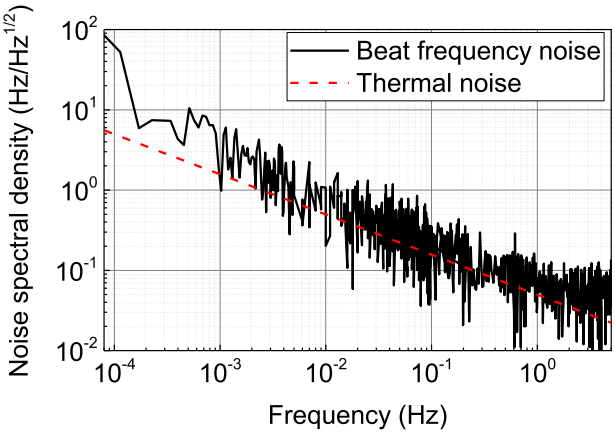

FIG. 10. Frequency noise of the beat between two Nd:YAG lasers stabilized by 20-cm optical cavities. The dashed line is the thermal noise resulting from two optical cavities.

measured to be 0.12 and 0.094 Hz (0.085 and 0.066 Hz for a single laser) with sampling times of T = 16 and 32 s, respectively. Showing the dependence of the linewidth on the sampling time, Fig. 11 is a summary of results from Ref. 30 and current investigation. In Fig. 11, all curves are the calculation using the simplified relationship and symbols are experimental values, including the two newly added data points. Figure 11 is divided into upper and lower regions by a straight line of $T \times f_m = 5$, and the approximation[30] used to obtain the relationship applies to the region above the line. Here, f_m is a characteristic frequency above which the noise components in the frequency domain do not affect the linewidth. The measured linewidths of both Nd:YAG lasers and the RF oscillator agree with the predication of the simplified relationship in the region of

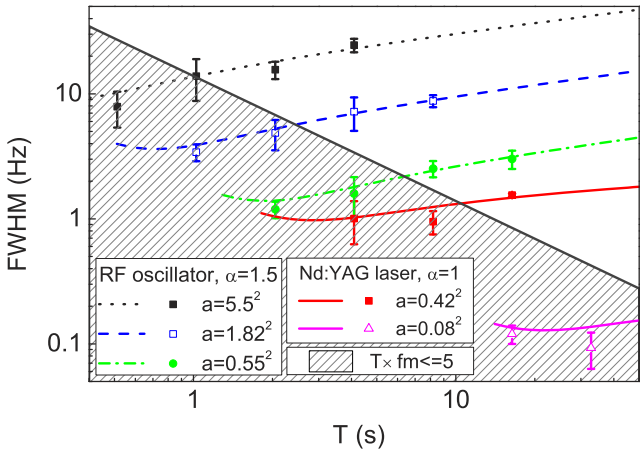

FIG. 11. Linewidth vs the sampling time T. The two data points (triangles) at the bottom are the current result. Symbols are the experimental data, and the corresponding curves are the calculations according to a simplified relationship[39] between the linewidth and the underlying frequency noise a/f^{α}. The hatched area indicates the parametric region that is not covered by the simplified model.

$T \times f_m > 5$, and there is still reasonable agreement outside the parametric coverage of the simplified relationship.

VI. CONCLUSION

We have developed two ultra-stable 1064-nm Nd:YAG NPRO lasers referenced to 20-cm optical cavities operated at room temperature. Silica mirror substrates are used for the optical cavity to reduce the thermal noise. The optical cavity and its support are optimized with the help of FEA modeling, and the measured acceleration sensitivities on the orders of 10^{-11} to 10^{-10}/g. The thermal stability of the vacuum chamber housing the optical cavity is improved to ~100 μK, and the time constant of the optical cavity is increased to ~70 h. Furthermore, the optical cavity is operated close to its zero-expansion temperature T_c. The frequency instability of the cavity-stabilized Nd:YAG laser reaches the minimum of 2.5×10^{-16} around 1 s and maintains at 10^{-16} level for averaging times up to 1000 s. The measured linewidth of the cavity-stabilized laser is 0.085 and 0.066 Hz with sampling times of 16 and 32 s, respectively, a time dependence that is consistent with the predication by a simplified model.[39] Technologies accumulated along with the development of the 20-cm-cavity project laid the foundation for ongoing projects on ultra-stable lasers for various applications such as optical frequency metrology, high-precision test of special relativity, and space-based gravitational wave observation.

ACKNOWLEDGMENTS

This work was supported by the National Basic Research Program of China (Grant No. 2012CB821303), the Strategic Priority Research Program of the Chinese Academy of Sciences (Grant Nos. XDA15020703, XDB21010300, and XDB23030202), the National Key R&D Program of China (Grant No. 2017YFA0304403), and the National Natural Science Foundation of China (Grant Nos. 11327407 and 11654004).

DATA AVAILABILITY

The data that support the findings of this study are available from the corresponding author upon reasonable request.

REFERENCES

[1] B. C. Young, F. C. Cruz, W. M. Itano, and J. C. Bergquist, Phys. Rev. Lett. **82**, 3799 (1999).
[2] M. Notcutt, L. Ma, J. Ye, and J. L. Hall, Opt. Lett. **30**, 1815 (2005).
[3] S. A. Webster, M. Oxborrow, S. Pugla, J. Millo, and P. Gill, Phys. Rev. A **77**, 033847 (2008).
[4] J. Alnis, A. Matveev, N. Kolachevsky, T. Udem, and T. W. Hänsch, Phys. Rev. A **77**, 053809 (2008).
[5] T. L. Nicholson, M. J. Martin, J. R. Williams, B. J. Bloom, M. Bishof, M. D. Swallows, S. L. Campbell, and J. Ye, Phys. Rev. Lett. **109**, 230801 (2012).
[6] S. Häfner, S. Falke, C. Grebing, S. Vogt, T. Legero, M. Merimaa, C. Lisdat, and U. Sterr, Opt. Lett. **40**, 2112 (2015).
[7] L. Wu, Y. Jiang, C. Ma, W. Qi, H. Yu, Z. Bi, and L. Ma, Sci. Rep. **6**, 24969 (2016).
[8] D. G. Matei, T. Legero, S. Häfner, C. Grebing, R. Weyrich, W. Zhang, L. Sonderhouse, J. M. Robinson, J. Ye, F. Riehle, and U. Sterr, Phys. Rev. Lett. **118**, 263202 (2017).

[9]W. Zhang, J. M. Robinson, L. Sonderhouse, E. Oelker, C. Benko, J. L. Hall, T. Legero, D. G. Matei, F. Riehle, U. Sterr, and J. Ye, Phys. Rev. Lett. **119**, 243601 (2017).
[10]L. Jin, Y. Jiang, Y. Yao, H. Yu, Z. Bi, and L. Ma, Opt. Express **26**, 18699 (2018).
[11]X. Y. Zeng, Y. X. Ye, X. H. Shi, Z. Y. Wang, K. Deng, J. Zhang, and Z. H. Lu, Opt. Lett. **43**, 1690 (2018).
[12]T. L. Nicholson, S. L. Campbell, R. B. Hutson, G. E. Marti, B. J. Bloom, R. L. McNally, W. Zhang, M. D. Barrett, M. S. Safronova, G. F. Strouse, W. L. Tew, and J. Ye, Nat. Commun. **6**, 6896 (2015).
[13]C. W. Chou, D. B. Hume, J. C. J. Koelemeij, D. J. Wineland, and T. Rosenband, Phys. Rev. Lett. **104**, 070802 (2010).
[14]S. L. Campbell, R. B. Hutson, G. E. Marti, A. Goban, N. Darkwah Oppong, R. L. McNally, L. Sonderhouse, J. M. Robinson, W. Zhang, B. J. Bloom, and J. Ye, Science **358**, 90 (2017).
[15]The LIGO Scientific Collaboration, Nat. Phys. **7**, 962 (2011).
[16]B. P. Abbott *et al.*, Phys. Rev. Lett. **116**, 061102 (2016).
[17]P. Bender and LISA Study Team, *Laser Interferometer Space Antenna for the Detection of Gravitational Waves*, Pre-Phase A Report, MPQ233 (Max-Planck-Institute for Quantum Optics, 1998).
[18]K. Danzmann and LISA Study Team, Adv. Space Res. **32**, 1233 (2003).
[19]M. Armano *et al.*, Phys. Rev. Lett. **116**, 231101 (2016).
[20]S. Kawamura *et al.*, Classical Quantum Gravity **23**, S125 (2006).
[21]J. Crowder and N. J. Cornish, Phys. Rev. D **72**, 083005 (2005).
[22]C. Eisele, A. Y. Nevsky, and S. Schiller, Phys. Rev. Lett. **103**, 090401 (2009).
[23]S. Herrmann, A. Senger, K. Möhle, M. Nagel, E. V. Kovalchuk, and A. Peters, Phys. Rev. D **80**, 105011 (2009).
[24]Q. Chen, E. Magoulakis, and S. Schiller, Phys. Rev. D **93**, 022003 (2016).
[25]K. Numata, A. Kemery, and J. Camp, Phys. Rev. Lett. **93**, 250602 (2004).
[26]J. Millo, D. V. Magalhães, C. Mandache, Y. Le Coq, E. M. L. English, P. G. Westergaard, J. Lodewyck, S. Bize, P. Lemonde, and G. Santarelli, Phys. Rev. A **79**, 053829 (2009).
[27]D. Jiao, J. Gao, X. Deng, G. Xu, J. Liu, T. Liu, R. Dong, and S. Zhang, Opt. Commun. **463**, 125460 (2020).
[28]G. D. Cole, W. Zhang, M. J. Martin, J. Ye, and M. Aspelmeyer, Nat. Photonics **7**, 644 (2013).
[29]G. D. Cole, W. Zhang, B. J. Bjork, D. Follman, P. Heu, C. Deutsch, L. Sonderhouse, J. Robinson, C. Franz, A. Alexandrovski, M. Notcutt, O. H. Heckl, J. Ye, and M. Aspelmeyer, Optica **3**, 647 (2016).
[30]L. Li, H. Shen, J. Bi, C. Wang, S. Lv, and L. Chen, Appl. Phys. B **117**, 1025 (2014).
[31]T. Kessler, C. Hagemann, C. Grebing, T. Legero, U. Sterr, F. Riehle, M. J. Martin, L. Chen, and J. Ye, Nat. Photonics **6**, 687 (2012).
[32]L. Chen, J. L. Hall, J. Ye, T. Yang, E. Zang, and T. Li, Phys. Rev. A **74**, 053801 (2006).
[33]D. R. Leibrandt, M. J. Thorpe, M. Notcutt, R. E. Drullinger, T. Rosenband, and J. C. Bergquist, Opt. Express **19**, 3471 (2011).
[34]J. Zhang, Y. Luo, B. Ouyang, K. Deng, Z. Lua, and J. Luo, Eur. Phys. J. D **67**, 46 (2013).
[35]K. L. Dooley, M. A. Arain, D. Feldbaum, V. V. Frolov, M. Heintze, D. Hoak, E. A. Khazanov, A. Lucianetti, R. M. Martin, G. Mueller, O. Palashov, V. Quetschke, D. H. Reitze, R. L. Savage, D. B. Tanner, L. F. Williams, and W. Wu, Rev. Sci. Instrum. **83**, 033109 (2012).
[36]Z. Li, W. Ma, W. Yang, Y. Wang, and Y. Zheng, Opt. Lett. **41**, 3331 (2016).
[37]Z. Tai, L. Yan, Y. Zhang, X. Zhang, W. Guo, S. Zhang, and H. Jiang, Opt. Lett. **41**, 5584 (2016).
[38]J. Bi, Y. Zhi, L. Li, and L. Chen, Appl. Opt. **58**, 690 (2019).
[39]G. Di Domenico, S. Schilt, and P. Thomann, Appl. Opt. **49**, 4801 (2010).
[40]R. W. P. Drever, J. L. Hall, F. V. Kowalski, J. Hough, G. M. Ford, A. J. Munley, and H. Ward, Appl. Phys. B **31**, 97 (1983).
[41]L. Ma, P. Jungner, J. Ye, and J. L. Hall, Opt. Lett. **19**, 1777 (1994).
[42]N. C. Wong and J. L. Hall, J. Opt. Soc. Am. B **2**, 1527 (1985).
[43]C. Ishibashi, J. Ye, and J. L. Hall, in *Quantum Electronics and Laser Science Conference*, edited by H. Gibbs, D. Wineland, D. Gammon, and D. Heinzen (OSA Technical Digest; Optical Society of America, 2002), p. QTuF27.
[44]L. Li, F. Liu, C. Wang, and L. Chen, Rev. Sci. Instrum. **83**, 043111 (2012).
[45]H. Shen, L. Li, J. Bi, J. Wang, and L. Chen, Phys. Rev. A **92**, 063809 (2015).
[46]R. W. Fox, Opt. Express **17**, 15023 (2009).
[47]T. Legero, T. Kessler, and U. Sterr, J. Opt. Soc. Am. B **27**, 914 (2010).
[48]J. Poirson, F. Bretenaker, M. Vallet, and A. Le Floch, J. Opt. Soc. Am. B **14**, 2811 (1997).
[49]L. Li, Y. Li, and L. Chen, Chin. J. Lasers **37**, 3075 (2010).
[50]C. J. Hood, H. J. Kimble, and J. Ye, Phys. Rev. A **64**, 033804 (2001).
[51]C. Hagemann, C. Grebing, C. Lisdat, S. Falke, T. Legero, U. Sterr, F. Riehle, M. J. Martin, and J. Ye, Opt. Lett. **39**, 5102 (2014).